changes in grey and white matter during adolescence. Neuroimage, 49:94-103.
[20] Giorgio A, Santelli L, Tomassini V, Bosnell R, Smith S, De Stefano N, et al. (2010). Age-related changes in grey and white matter structure throughout adulthood. Neuroimage, 51:943-51.
[21] Streitbürger DP, Möller HE, Tittgemeyer M, Hund-Georgiadis M, Schroeter ML, Mueller K (2012). Investigating structural brain changes of dehydration using voxel-based morphometry. PLoS One, 7:e44195.
[22] Hutton C, Draganski B, Ashburner J, Weiskopf N (2009). A comparison between voxel-based cortical thickness and voxel-based morphometry in normal aging. Neuroimage, 48:371-80.
[23] Braak H, Braak E (1995). Staging of Alzheimer's disease-related neurofibrillary changes. Neurobiol Aging,16:271-8.
[24] Ohnishi T, Matsuda H, Tabira T, Asada T, Uno M (2001). Changes in brain morphology in Alzheimer disease and normal aging: is Alzheimer disease an exaggerated aging process? AJNR Am J Neuroradiol, 22:1680-5.
[25] Matsuda H, Kitayama N, Ohnishi T, Asada T, Nakano S, Sakamoto S, et al. (2002). Longitudinal evaluation of both morphologic and functional changes in the same individuals with Alzheimer's disease. J Nucl Med,43:304-11.
[26] Chetelat G, Desgranges B, de la Sayette V, Viader F, Berkouk K, Landeau B, et al. (2003). Dissociating atrophy and hypometabolism impact on episodic memory in mild cognitive impairment. Brain, 126:1955-67.
[27] Rémy F, Mirrashed F, Campbell B, Richter W (2005). Verbal episodic memory impairment in Alzheimer's disease: a combined structural and functional MRI study. Neuroimage,25:253-66.
[28] Hirata Y, Matsuda H, Nemoto K, Ohnishi T, Hirao K, Yamashita F, et al. (2005). Voxel-based morphometry to discriminate early Alzheimer's disease from controls. Neurosci Lett,382:269-74.
[29] Di Paola M, Macaluso E, Carlesimo GA, Tomaiuolo F, Worsley KJ, Fadda L, et al. (2007). Episodic memory impairment in patients with Alzheimer's disease is correlated with entorhinal cortex atrophy. A voxel-based morphometry study. J Neurol, 254:774-81.
[30] Hämäläinen A, Pihlajamäki M, Tanila H, Hänninen T, Niskanen E, Tervo S, et al. (2007). Increased fMRI responses during encoding in mild cognitive impairment. Neurobiol Aging, 28:1889-903.
[31] Leube DT, Weis S, Freymann K, Erb M, Jessen F, Heun R, et al. (2008). Neural correlates of verbal episodic memory in patients with MCI and Alzheimer's disease--a VBM study. Int J Geriatr Psychiatry,23:1114-8.
[32] Schmidt-Wilcke T, Poljansky S, Hierlmeier S, Hausner J, Ibach B (2009). Memory performance correlates with gray matter density in the ento-/perirhinal cortex and posterior hippocampus in patients with mild cognitive impairment and healthy controls--a voxel based morphometry study. Neuroimage, 47:1914-20.
[33] Goto M, Abe O, Miyati T, Yoshikawa T, Hayashi N, Takao H, et al. (2011). Entorhinal cortex volume measured with 3T MRI is positively correlated with the Wechsler Memory Scale-Revised logical/verbal memory score for healthy subjects. Neuroradiology, 53:617-22.
[34] Chételat G, Villemagne VL, Pike KE, Ellis KA, Bourgeat P, Jones G, et al. (2011). Independent contribution of temporal beta-amyloid deposition to memory decline in the pre-dementia phase of Alzheimer's disease. Brain, 134:798-807.
[35] Nho K, Risacher SL, Crane PK, Decarli C, Glymour MM, Habeck C, et al.(2012). Voxel and surface-based topography of memory and executive deficits in mild cognitive impairment and Alzheimer's disease. Brain Imaging Behav, DOI 10.1007/s11682-012-9203-2
[36] Whitwell JL, Dickson DW, Murray ME, Weigand SD, Tosakulwong N, Senjem ML, et al. (2012). Neuroimaging correlates of pathologically defined subtypes of Alzheimer's disease: a case-control study. Lancet Neurol,11:868-77.
[37] Ishii K, Kawachi T, Sasaki H, Kono AK, Fukuda T, Kojima Y,et al. (2005). Voxel-based morphometric comparison between early- and late-onset mild Alzheimer's disease and assessment of diagnostic performance of z score images. AJNR Am J Neuroradiol, 26:333-40.
[38] Matsunari I, Samuraki M, Chen WP, Yanase D, Takeda N, Ono K et al. (2007). Comparison of ^{18}F-FDG PET and optimized voxel-based morphometry for detection of Alzheimer's disease: aging effect on diagnostic performance. J Nucl Med, 2007;48:1961-70.
[39] Frisoni GB, Pievani M, Testa C, Sabattoli F, Bresciani L, Bonetti M, et al.(2007). The topography of grey matter involvement in early and late onset Alzheimer's disease. Brain, 2007;130:720-30.
[40] Li J, Pan P, Huang R, Shang H (2012). A meta-analysis of voxel-based morphometry studies of white matter volume alterations in Alzheimer's disease. Neurosci Biobehav Rev,36:757-63.
[41] Testa C, Laakso MP, Sabattoli F, Rossi R, Beltramello A, Soininen H, et al.(2004). A comparison between the accuracy of voxel-based morphometry and hippocampal volumetry in Alzheimer's disease. J Magn Reson Imaging,19:274-82.
[42] Matsuda H, Mizumura S, Nemoto K, Yamashita F, Imabayashi E, Sato N, et al. (2012). Automatic voxel-based morphometry of structural MRI by SPM8 plus diffeomorphic anatomic registration through exponentiated lie algebra improves the diagnosis of probable Alzheimer Disease. AJNR Am J Neuroradiol,33:1109-14.

NeuroImage: Clinical 2 (2013) 491–496

Contents lists available at SciVerse ScienceDirect

NeuroImage: Clinical

journal homepage: www.elsevier.com/locate/ynicl

In vivo evaluation of gray and white matter volume loss in the parkinsonian variant of multiple system atrophy using SPM8 plus DARTEL for VBM ☆

Yoko Shigemoto [a], Hiroshi Matsuda [b,*], Kouhei Kamiya [a], Norihide Maikusa [b], Yasuhiro Nakata [a], Kimiteru Ito [a], Miho Ota [c], Naofumi Matsunaga [d], Noriko Sato [a]

[a] Department of Radiology, National Center Hospital of Neurology and Psychiatry, 4-1-1 Ogawahigashi, Kodaira, Tokyo 187-8551 Japan
[b] Integrative Brain Imaging Center, National Center of Neurology and Psychiatry, 4-1-1 Ogawahigashi, Kodaira, Tokyo 187-8551 Japan
[c] Department of Mental Disorder Research, National Institute of Neuroscience, National Center of Neurology and Psychiatry, 4-1-1 Ogawa-Higashi, Kodaira, Tokyo 187-8502, Japan
[d] Department of Radiology, Yamaguchi University Graduate School of Medicine, 1-1-1 Minamikogushi, Ube, Yamaguchi 755-8505, Japan

ARTICLE INFO

Article history:
Received 5 January 2013
Received in revised form 26 March 2013
Accepted 27 March 2013
Available online xxxx

Keywords:
Multiple system atrophy with predominant parkinsonism (MSA-P)
White matter
Diffeomorphic anatomical registration through exponentiated Lie algebra (DARTEL)
Statistical parametric mapping (SPM)
Voxel-based morphometry (VBM)

ABSTRACT

In multiple system atrophy with predominant parkinsonism (MSA-P), several voxel-based morphometry (VBM) studies have revealed gray matter loss; however, the white matter volume changes have been rarely reported. We investigated the volume changes of white matter as well as gray matter by VBM. A retrospective MRI study was performed in 20 patients with MSA-P and 30 age-matched healthy controls. We applied VBM with statistical parametric mapping (SPM8) plus diffeomorphic anatomical registration through exponentiated Lie algebra (DARTEL) to explore the regional atrophy of gray and white matter in all of the MSA-P patients, 14 patients with left-side dominant and 6 patients with right-side dominant onset as compared to controls. In all of the MSA-P patients, VBM revealed a significant volume reduction of gray matter in the bilateral putamina, cerebellums and dorsal midbrain. White matter loss was located in bilateral globus pallidi, external capsules extending to the midbrain, right subcortical to precentral area through internal capsule, the pons, bilateral middle cerebellar peduncles and left cerebellum. In left-side dominant MSA-P patients, the gray and white matter volume loss was detected predominantly on the right side and vice versa in right-side dominant MSA-P patients. A correlation with disease duration and severity was not detected. VBM using SPM8 plus DARTEL detected significant volume loss not only in the gray but also in the white matter of the area affected by MSA-P.

1. Introduction

MSA is a sporadic, progressive, neurodegenerative disorder clinically characterized by autonomic dysfunction, parkinsonism, cerebellar ataxia, and pyramidal signs (Quinn, 1989). MSA can be classified into two subgroups, a cerebellar (MSA-C) and a parkinsonian (MSA-P) variant (Gilman et al., 2008). Neuropathologically, MSA is characterized by selective neuronal loss and reactive gliosis predominantly affecting the basal ganglia, substantia nigra, olivopontocerebellar pathways and the intermediolateral cell column of the spinal cord (Papp and Lantos, 1994; Wenning et al., 1997). The histological hallmarks of MSA are α-synuclein-positive glial cytoplasmic inclusions in the oligodendroglia, which are required for the diagnosis of definite MSA (Gilman et al., 2008; Papp and Lantos, 1994; Wenning et al., 1997).

VBM is a method of statistically analyzing morphological changes in the brain as measured by whole-brain MRI data (Ashburner and Friston, 2000). In the past few years, VBM has been used to study the patterns of structural changes in the brain during brain development or in neurodegenerative disorders (Bergfield et al., 2010; Brenneis et al., 2004; Burton et al., 2002). In MSA-P, VBM revealed gray matter loss mainly in the striatum, the cerebral cortex including the motor area and the cerebellar lobes (Brenneis et al., 2003, 2007; Minnerop et al., 2007; Tir et al., 2009; Tzarouchi et al., 2010). However, white matter volume changes have been rarely reported, and the results were inconsistent (Brenneis et al., 2003; Minnerop et al., 2007, 2010; Tzarouchi et al., 2010).

In the present study, we evaluated MR images of MSA-P patients to examine the volume changes of white matter as well as gray matter by using the latest VBM technique with SPM 8 plus DARTEL (Matsuda et al., 2012).

* Corresponding author at: 4-1-1 Ogawahigashi, Kodaira, Tokyo 187-8551, Japan. Tel.: +81 42 341 2712x2171; fax: +81 42 346 2229.
E-mail address: matsudah@ncnp.go.jp (H. Matsuda).

2213-1582/$ – see front matter © 2013 The Authors. Published by Elsevier Inc. All rights reserved.
http://dx.doi.org/10.1016/j.nicl.2013.03.017

2. Materials and methods

2.1. Participants

We retrospectively reviewed an electronic database of radiology reports for 12,029 patients who underwent brain MRI examinations at our institution between March 2007 and September 2010 and searched for reports that indicated Parkinson's disease and related disorders. After 127 patients were indicated by the radiological reports, medical records revealed 23 patients who were diagnosed as possible or probable MSA-P according to consensus criteria (Gilman et al., 2008). Among 23 patients, three patients were excluded because of the presence of multiple lacunar infarctions in two patients and multiple cavernous hemangiomas in one patient. All volumetric T1-weighted images were visually inspected for apparent artifacts due to patient motion or metallic dental prostheses. As a consequence, 20 patients (7 men and 13 women; age range 48–77 years, mean age 62.9 ± 7.7 years, disease duration 4.1 ± 2.2 years) were enrolled as subjects in this study. The patient data are given in Table 1. Among these patients, 14 patients had left-side dominant (5 men and 9 women; age range 53–77 years, mean age 64.1 ± 6.4 years, disease duration 4.2 ± 2.5 years) and 6 patients had right-side dominant onset symptoms (2 men and 4 women; age range 48–73 years, mean age 59.8 ± 10.0 years, disease duration 3.7 ± 1.2 years). As a measure of disease severity, we adopted the following disease stages previously described: stage 0 = no gait difficulties, stage 1 = disease onset, as defined by onset of gait difficulties, stage 2 = loss of independent gait, as defined by permanent use of a walking aid or reliance on a supporting arm, stage 3 = confinement to wheelchair, as defined by permanent use of a wheelchair (Klockgether et al., 1998).

Our local ethics committee did not require approval or patient informed consent for the retrospective review. Thirty age-matched control subjects (10 men and 20 women; age range 48–80 years, mean age 64.7 ± 7.7 years) were also involved as healthy control subjects.

Thirty age-matched healthy controls (10 men and 20 women; age range 48–80 years, mean age 64.7 ± 7.7 years) were also involved as control subjects. None had a history of neurological or psychiatric illness, and no abnormalities were observed on their brain structural MRIs. Institutional review board approval and written informed consent were obtained from the control subjects.

2.2. Image acquisition and analysis

All examinations were performed with a 1.5 T MR imaging system (Symphony Vision; Siemens, Erlangen, Germany). MR protocol for the parkinsonian is as follows. High-resolution three-dimensional (3D) T1-weighted images were acquired using magnetization-prepared rapid acquisition of a gradient echo sequence (144 sagittal sections, TR = 1600 ms, TE = 2.6 ms, flip angle = 15°, voxel size = 1.2 × 1.2 × 1.2 mm^3, FOV = 315 mm, matrix = 208 × 256, 1.2-mm thickness with no gap). Axial T2-weighted images (TR = 3800 ms, TE = 95 ms, flip angle = 150°, voxel size = 0.7 × 0.4 × 5.0 mm^3, FOV = 230 mm, matrix = 281 × 512, 5-mm thickness with 1.8-mm gap) and coronal fluid attenuation inversion recovery images (TR = 9000 ms, TE = 100 ms, flip angle = 170°, voxel size = 1.2 × 0.9 × 5.0 mm^3, FOV 230 mm, matrix = 192 × 256, 5.0-mm thickness with 1.8-mm gap) were also obtained.

Using the latest version of SPM8 (Wellcome Department of Imaging Neuroscience, London, United Kingdom), we segmented the MRIs into gray matter, white matter, and cerebrospinal fluid images by a unified tissue-segmentation procedure after image-intensity nonuniformity correction. These segmented gray and white matter images were then spatially normalized to the customized template in the standardized anatomic space by using DARTEL (Wellcome Department of Imaging Neuroscience) (Ashburner, 2007). To preserve the gray and white matter volumes within each voxel, we modulated the images using the Jacobean determinants derived from the spatial normalization by DARTEL and then smoothed them using an 8-mm FWHM Gaussian kernel.

Morphological group differences for these smoothed gray and white matter images between all of the MSA-P patients and the controls were analyzed using a 2-sample *t*-test in SPM8. The same analysis was performed between the 14 left-side dominant onset MSA-P patients and the controls and between the 6 right-side dominant onset MSA-P patients and the controls. Group comparisons by SPM8 were assessed using the false discovery rate at a threshold of $p < .05$, corrected for multiple comparisons.

Additionally, for the correlation analyses with disease duration and disease stage, we used a multiple regression analysis and an uncorrected threshold of $p < .001$.

3. Results

In MSA-P patients, VBM revealed regions of gray matter loss bilaterally affecting the putamina, cerebellums, dorsal midbrain and left inferior occipital gyrus (see Table 2, Fig. 1). Reduced white matter volume was located in the bilateral globus pallidi and external capsules extending to the midbrain (see Table 3, Fig. 2). On the right side, it extended upward to the subcortical to precentral area through the internal capsule. White matter loss in the pons, bilateral middle cerebellar peduncles and left cerebellum was also detected. In left-side dominant MSA-P patients, the putaminal gray matter was decreased only on the right side (see Table 4, Fig. 3). The reduced white matter was located in the right globus pallidus and external capsule (see Table 5, Fig. 3). In right-side dominant MSA-P patients, gray matter was reduced in the left putamen, bilateral cerebellums

Table 1
Demographic characteristics of MSA-P patients and controls.

Characteristic	MSA-P	Controls
Age (y)	62.9 ± 7.7 (48–77)	62.9 ± 7.7 (48–80)
Sex	7 men, 13 women	10 men, 20 women
Diagnosis	16 probable MSA-P, 4 possible MSA-P	
Disease duration (y)	4.1 ± 2.2 (2–10)	
Stage 1	6	
Stage 2	11	
Stage 3	3	
Cerebellar symptoms	7 present, 13 absent	
Pyramidal signs	7 present, 13 absent	
Urinary incontinence	15 present, 5 absent	
Orthostatic hypotension	13 present, 7 absent	

Note: Unless otherwise indicated, data are means ± standard deviations, with ranges in parentheses. Stage 0 = no gait difficulties, stage 1 = disease onset, as defined by onset of gait difficulties, stage 2 = loss of independent gait, as defined by permanent use of a walking aid or reliance on a supporting arm, stage 3 = confinement to wheelchair, as defined by permanent use of a wheelchair.

Table 2
Clusters of gray matter loss (20 MSA-P vs. 30 controls).

Region volume (mm^3)	Z score	Talairach coordinates (x, y, z)	Location of local maxima
9680	4.46	40, −46, −36	Right cerebellar tonsil
	3.79	36, −69, −15	Right cerebellum
	3.55	24, −46, −13	Right cerebellum
8424	6.36	26, 14, 7	Right putamen
6960	4.31	−40, −54, −23	Left cerebellum
	3.6	−28, −84, −9	Left inferior occipital gyrus
	3.31	−20, −75, −20	Left cerebellum
5712	6.05	−26, 8, 7	Left putamen
3896	4.6	0, −34, −12	Dorsal midbrain

Voxel size 2 × 2 × 2 mm^3. Clusters of gray matter SPM analysis with FDR-corrected at $p < .05$ are shown. The coordinates refer to the Talairach reference space.

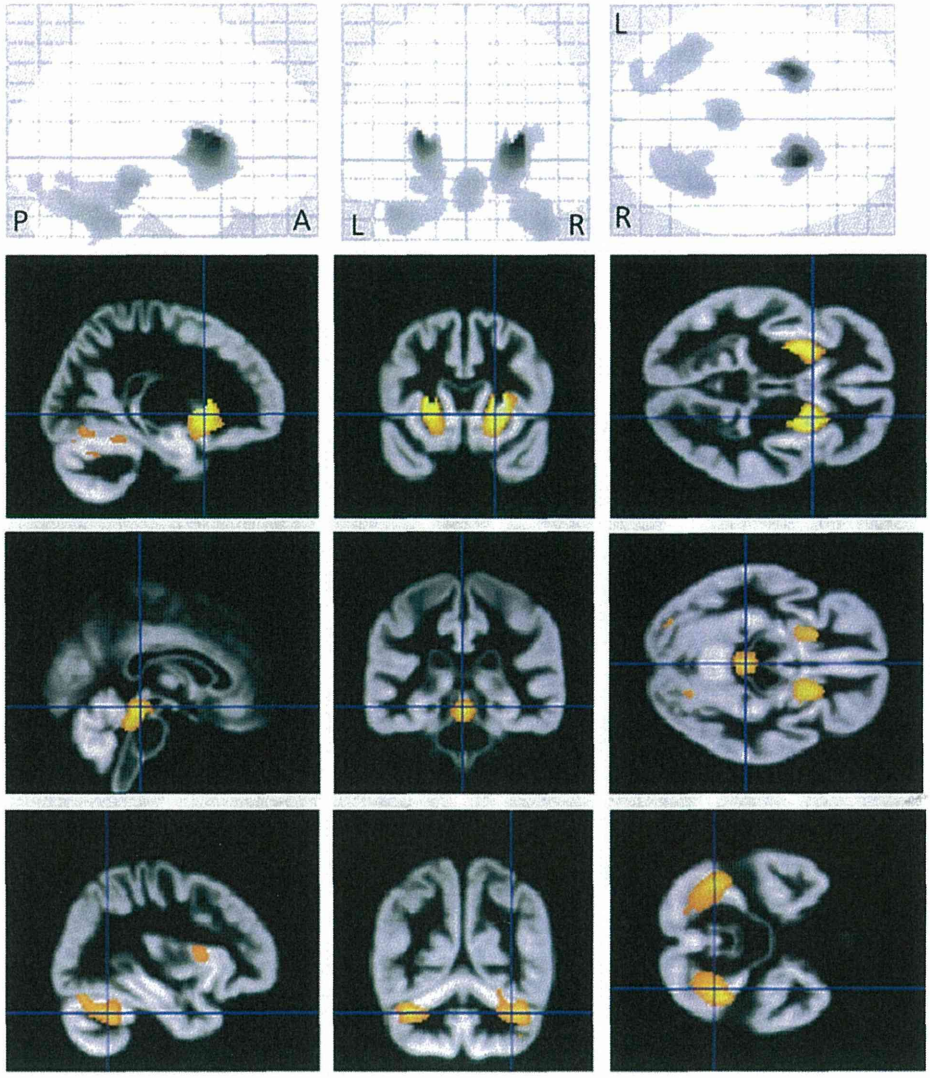

Fig. 1. Comparison of gray matter volume by VBM using SPM8 plus DARTEL among 20 patients with MSA-P and 30 control subjects. Significant atrophy is observed in the bilateral putamina, cerebellums, dorsal midbrain and left inferior occipital gyrus in MSA-P patients compared to controls. Results are superimposed on the customized gray matter template (FDR-corrected at $p < .05$).

and several cortical regions (see Table 6, Fig. 4). The reduced white matter was located in the left globus pallidus, bilateral external capsules, right frontal lobe, right parahippocampal area and right cerebellum (see Table 7, Fig. 4). A correlation with disease duration and severity was not detected.

Table 3
Clusters of white matter loss (20 MSA-P vs. 30 controls).

Region volume (mm^3)	Z score	Talairach coordinates (x, y, z)	Location of local maxima
32,144	4.23	−12, −64, −34	Left cerebellum
	4.12	−16, −27, −32	Left pons
	4.07	−16, −38, −22	Left cerebellum
20,360	5.46	32, −10, 2	Right external capsule
	4.94	18, 2, −5	Right lateral globus pallidus
	3.35	36, −6, 32	Right sub-precentral area
10,272	5.04	−34, −8, 4	Left external capsule
	4.79	−20, −2, −5	Left lateral globus pallidus

Voxel size 2 × 2 × 2 mm^3. Clusters of gray matter SPM analysis with FDR-corrected at $p < .05$ are shown. The coordinates refer to the Talairach reference space.

4. Discussion

To our knowledge, this is the first study to focus on the white matter volume loss in MSA-P patients as determined by VBM using SPM8 plus DARTEL. This analysis showed white matter atrophy in the globus pallidi and external capsules bilaterally extending to the midbrain. The white matter atrophy also spreads upward to the subcortical to right premotor area. These areas correspond to the regions connecting the pathologically affected structures. Such findings, which seemed to reflect the degeneration of the motor pathway, have never been presented in previous VBM studies. We believe that the evaluation of white matter as well as deep gray matter has significantly improved owing to this new software.

Neuropathological studies have shown neuronal loss and reactive gliosis in the putamen, caudate nucleus, external pallidum, substantia nigra, locus coeruleus, inferior olives, pontine nuclei, cerebellar lobes and intermediolateral cell columns of the spinal cord in MSA-P (Wenning et al., 1997). Most severe neuronal loss was found in the lateral part of the substantia nigra and dorsolateral putamen (Jellinger et al., 2005; Ozawa et al., 2004; Wenning et al., 2002). The previous VBM studies have reported gray matter loss in the putamen, caudate nucleus,

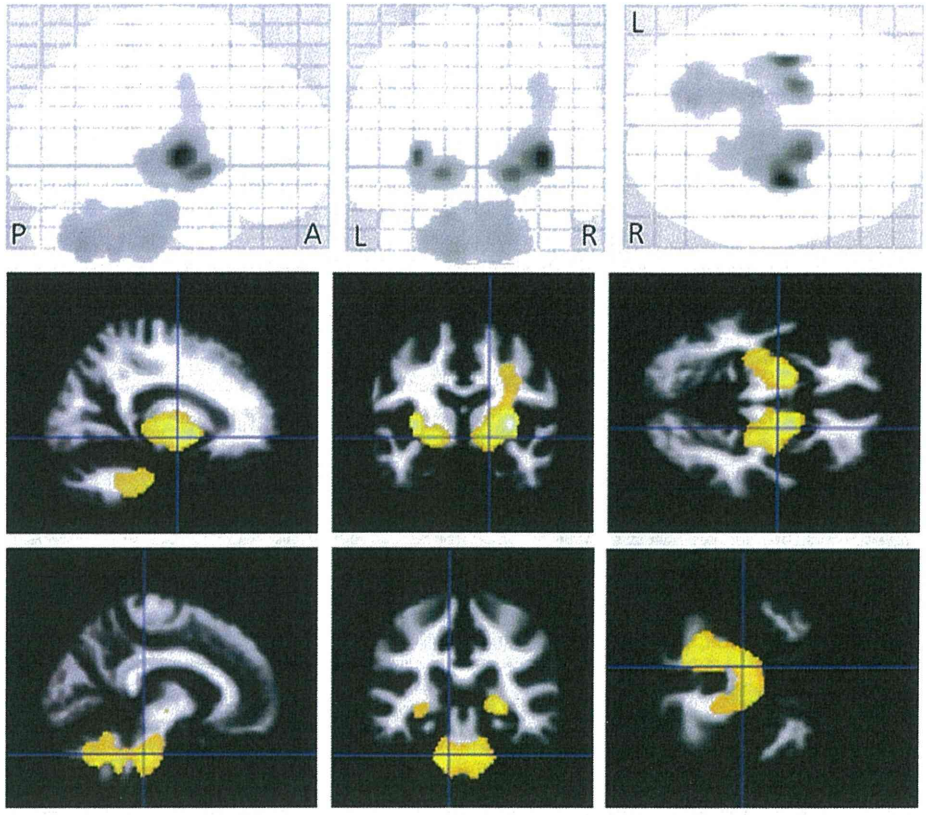

Fig. 2. Comparison of white matter volume by VBM using SPM8 plus DARTEL among 20 patients with MSA-P and 30 control subjects. Significant atrophy is observed in the bilateral globus pallidi and external capsules extending to the midbrain. On the right side, the atrophy extends upward to the subcortical to precentral area through the internal capsule. White matter atrophy in the pons, bilateral middle cerebellar peduncles and left cerebellum is also detected. Results are superimposed on the customized white matter template (FDR-corrected at $p < .05$).

Table 4
Clusters of gray matter loss (14 left-side dominant onset MSA-P vs. 30 controls).

Region volume (mm^3)	Z score	Talairach coordinates (x, y, z)	Location of local maxima
6864	6.38	26, 14, 5	Right putamen

Voxel size $2 \times 2 \times 2$ mm^3. Clusters of gray matter SPM analysis with FDR-corrected at $p < .05$ are shown. The coordinates refer to the Talairach reference space.

cerebellar vermis and lobes, dorsal midbrain, and several cortical regions including the insular cortex and motor area (Brenneis et al., 2003, 2007; Chang et al., 2009; Minnerop et al., 2007, 2010; Tir et al., 2009; Tzarouchi et al., 2010). The significant putaminal loss detected in our study confirmed the findings of previous region of interest based morphometric and VBM studies (Brenneis et al., 2003, 2007; Minnerop et al., 2007; Schulz et al., 1999; Tzarouchi et al., 2010). Our VBM results also agree with the pathological features (Jellinger et al., 2005; Ozawa et al., 2004; Wenning et al., 1997, 2002).

Though some previous VBM studies have detected the atrophy of the caudate nucleus (Brenneis et al., 2003; Chang et al., 2009; Tzarouchi et al., 2010), our study did not detect volume loss in the caudate nucleus. Pathologically, the caudate nucleus is less involved than the putamen and tends to be relatively preserved in the early stage of MSA-P (Ozawa et al., 2004; Wenning et al., 2002). (Chang et al., 2009) reported that the caudate nucleus had significant atrophy compared to the putamen, a finding that is inconsistent with pathological features mentioned above. It is possible that the localization of deep gray matter at the periventricular space made it difficult to segment the MRIs in older versions of SPM. The recent report of Messina et al. (2011) supported our finding of no significant volume loss in the caudate nucleus as measured automatically by FreeSurfer.

Gray matter volume loss in the olivopontocerebellar system can also be seen in MSA-P, although the degree of involvement is lower

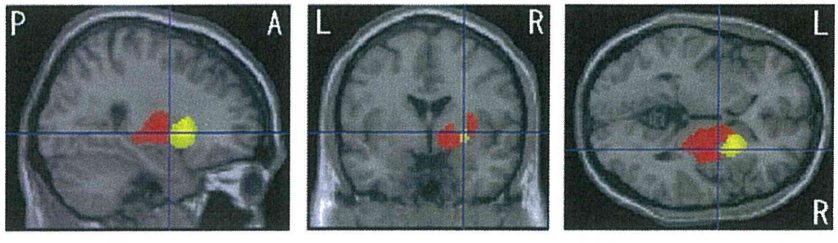

Fig. 3. Comparison of gray and white matter volumes by VBM using SPM8 plus DARTEL among 14 patients with left-side dominant onset MSA-P and 30 control subjects. Significant gray matter atrophy which is shown in a yellow color is observed only on the right side of the putamen (FDR-corrected at $p < .05$). Significant white matter atrophy which is shown in a red color is observed only on the right side of the globus pallidus and external capsule (FDR-corrected at $p < .05$).

Table 5
Clusters of white matter loss (14 left-side dominant onset MSA-P vs. 30 controls).

Voxel size 2 × 2 × 2 mm^3. Clusters of gray matter SPM analysis with FDR-corrected at $p < .05$ are shown. The coordinates refer to the Talairach reference space.

Region volume (mm^3)	Z score	Talairach coordinates (x, y, z)	Location of local maxima
13,448	5.51	32, −8, 4	Right external capsule
	4.93	18, 0, −5	Right lateral globus pallidus

Table 6
Clusters of gray matter loss (6 right-side dominant onset MSA-P vs. 30 controls).

Region volume (mm^3)	Z score	Talairach coordinates (x, y, z)	Location of local maxima
11,832	5.76	−27, 6, 5	Left putamen
	3.76	−61, −5, 8	Left superior temporal gyrus
	3.70	−36, −9, 13	Left insula
11,216	4.84	12, −7, 45	Right cingulate gyrus
	4.52	2, 17, 34	Right cingulate gyrus
	4.18	−12, −8, 43	Left cingulate gyrus
5536	3.76	20, −70, −8	Right lingual gyrus
	3.62	24, −76, −11	Right fusiform gyrus
	3.55	38, −54, −26	Right cerebellum
4504	3.86	−18, −86, −11	Left fusiform gyrus
	3.50	−36, −58, −24	Left cerebellum

Voxel size 2 × 2 × 2 mm^3. Clusters of gray matter SPM analysis with FDR-corrected at $p < .05$ are shown. The coordinates refer to the Talairach reference space.

than in MSA-C (Wenning et al., 1996, 1997). Atrophy of the cerebellar vermis and lobes was detected, which is in line with previous VBM studies (Chang et al., 2009; Minnerop et al., 2010; Tzarouchi et al., 2010) and pathological findings (Wenning et al., 1997). White matter cerebellar atrophy was also detected in addition to gray matter atrophy. The pons, bilateral middle cerebellar peduncles and the left cerebellar lobe were involved, a finding that was also consistent with previous VBM studies (Minnerop et al., 2010; Tzarouchi et al., 2010).

The white matter loss was detected in bilateral globus pallidi and external capsules extending to the midbrain which has never been reported before in a study using VBM. The white matter volume loss of the globus pallidus might reflect the fact that the globus pallidus has many efferent fibers and many bundles of myelinated fibers from the striatum traverse globus pallidus (Mamata et al., 2002; Nieuwenhuys et al., 2008). It is supported by the fact that the glucose metabolism of the globus pallidus is generally almost equal to white matter metabolism.

The areas connecting the globus pallidus with each structure were also significantly atrophic in this study. The neuronal loss in globus pallidus is pathologically proven (Jellinger et al., 2005; Ozawa et al., 2004; Wenning et al., 1997, 2002) and it plays an important role in parkinsonism as well as substantia nigra. Thus, those findings could result from the degeneration of the motor pathway such as striopallidal fiber, strionigral fiber and pallidonigral fiber (Nieuwenhuys et al., 2008). On the right side, the white matter volume loss extended upward to the subcortical to precentral area. The involvement of the precentral area could be explained by the fact that the motor cortex, the supplementary motor cortex and the premotor area were also involved in the pathways mentioned above; the afferent fibers of the striatum originate mainly from the motor and premotor areas, and then go back to the area (Nieuwenhuys et al., 2008). Another possibility is that the corticospinal tract itself is affected by this disease. The recent VBM studies of Minnerop et al. (2010) revealed white matter reduction along the corticospinal tract in the bilateral internal capsules and subcortical to left precentral gyrus, findings that agree with our study. However, they did not detect white matter atrophy around the deep gray matter. We believe that this was because they evaluated MSA patients including both MSA-C and MSA-P patients, and MSA-C patients made up more than 70% of their patient groups.

Table 7
Clusters of white matter loss (6 right-side dominant onset MSA-P vs. 30 controls).

Region volume (mm^3)	Z score	Talairach coordinates (x, y, z)	Location of local maxima
101,384	6.05	−34, −10, 2	Left external capsule
	5.68	−22, −6, −6	Left lateral globus pallidus
	4.79	22, −49, −19	Right cerebellum
4912	4.06	22, −32, 0	Right external capsule
	3.88	34, −12, 2	Right external capsule
	3.65	24, −8, −10	Right parahippocampal area
4288	4.08	30, 5, 26	Right frontal lobe
	3.97	46, 5, 20	Right frontal lobe
	3.71	28, −2, 41	Right frontal lobe

Voxel size 2 × 2 × 2 mm^3. Clusters of gray matter SPM analysis with FDR-corrected at $p < .05$ are shown. The coordinates refer to the Talairach reference space.

This better detection of deep gray matter and white matter volume loss in our study probably resulted from the application of the SPM8 plus DARTEL algorithm (Matsuda et al., 2012). The latest version of SPM8 enabled more accurate segmentation of the MRIs into gray matter, white matter, and cerebrospinal fluid images compared to older versions of SPM. In addition, DARTEL provides improved registration accuracy compared with conventional VBM.

In this study, we also evaluated both 14 left-side dominant and 6 right-side dominant onset MSA-P patients and detected the contralateral putaminal atrophy. Our results agreed with the previous MR imaging and pathological findings (Fearnley and Lees, 1990; Kato et al., 1992; Kume et al., 1992). The reduced white matter was also predominant in the contralateral globus pallidus and external capsule extending to the level of the midbrain. To our knowledge, this is also the first report to mention the laterality of the clinical findings and of white matter volume loss using VBM. The detection of volume loss only on the right side in the corona radiate of 20 MSA-P patients might be due to the large number of left-side dominant patients.

This study has several limitations. First, the number of patients in this study was not large. This might be the main reason for the failure

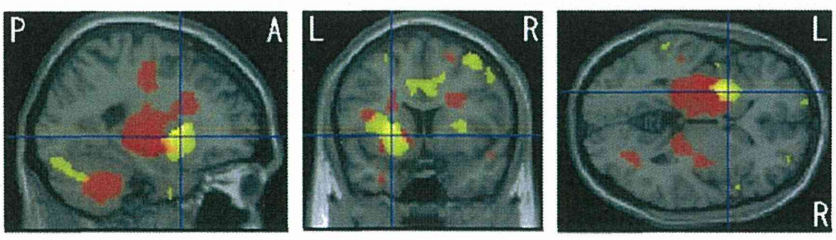

Fig. 4. Comparison of gray and white matter volumes by VBM using SPM8 plus DARTEL among 6 patients with right-side dominant onset MSA-P and 30 control subjects. Significant gray matter atrophy which is shown in a yellow color is observed in the left putamen, bilateral cerebellums and several cortical regions (FDR-corrected at $p < .05$). Bilateral cerebellums and several cortical regions are partly shown. Significant white matter atrophy which is shown in a red color is observed in the left globus pallidus, bilateral external capsules, right frontal lobe, parahippocampal area and cerebellum (FDR-corrected at $p < .05$).

of detecting the correlation with disease duration and severity. A few previous VBM studies with a small number of patients have reported inconsistent results on correlation with disease duration and severity (Brenneis et al., 2007; Minnerop et al., 2007, 2010). A further study with a large number of MSA-P patients would be necessary. Second, this study lacked the pathologic confirmation. However, it was difficult to select data only for pathologically confirmed patients, and the diagnosis in this study was clinically evaluated by an experienced neurologist based on consensus criteria. Third, we failed to detect the gray matter volume loss of the substantia nigra as well as in previous VBM studies, although the neuronal loss of substantia nigra is a hallmark of MSA-P (Mamata et al., 2002; Minnerop et al., 2010; Tir et al., 2009). Even though the software used for the analysis and the evaluation of spatial resolution have greatly improved, the segmentation of MRIs of nuclei located in brainstem remains a weakness.

5. Conclusions

In conclusion, VBM using SPM8 plus DARTEL detected significant volume loss not only in the gray but also in the white matter of the area affected by MSA-P. Significant structural atrophic change of the areas connecting the globus pallidus with each structure which plays a crucial role in parkinsonism was detected for the first time using VBM. Further prospective investigations involving a larger number of MSA-P patients combined with DTI techniques are required to confirm our findings. VBM using SPM8 plus DARTEL could also be a useful tool for evaluating other neurodegenerative diseases as well as MSA-P.

References

Ashburner, J., 2007. A fast diffeomorphic image registration algorithm. NeuroImage 38, 95–113.

Ashburner, J., Friston, K.J., 2000. Voxel-based morphometry: the methods. NeuroImage 11, 805–821.

Bergfield, K.L., Hanson, K.D., Chen, K., Teipel, S.J., Hampel, H., Rapoport, S.I., Moeller, J.R., Alexander, G.E., 2010. Age-related networks of regional covariance in MRI gray matter: reproducible multivariate patterns in healthy aging. NeuroImage 49, 1750–1759.

Brenneis, C., Seppi, K., Schocke, M.F., Müller, J., Luginger, E., Bösch, S., Löscher, W.N., Büchel, C., Poewe, W., Wenning, G.K., 2003. Voxel-based morphometry detects cortical atrophy in the Parkinson variant of multiple system atrophy. Movement Disorders 18, 1132–1138.

Brenneis, C., Seppi, K., Schocke, M., Benke, T., Wenning, G.K., Poewe, W., 2004. Voxel based morphometry reveals a distinct pattern of frontal atrophy in progressive supranuclear palsy. Journal of Neurology, Neurosurgery, and Psychiatry 75, 246–249.

Brenneis, C., Egger, K., Scherfler, C., Seppi, K., Schocke, M., Poewe, W., Wenning, G.K., 2007. Progression of brain atrophy in multiple system atrophy. A longitudinal VBM study. Journal of Neurology 254, 191–196.

Burton, E.J., Karas, G., Paling, S.M., Barber, R., Williams, E.D., Ballard, C.G., McKeith, I.G., Scheltens, P., Barkhof, F., O'Brien, J.T., 2002. Patterns of cerebral atrophy in dementia with Lewy bodies using voxel-based morphometry. NeuroImage 17, 618–630.

Chang, C.C., Chang, Y.Y., Chang, W.N., Lee, Y.C., Wang, Y.L., Lui, C.C., Huang, C.W., Liu, W.L., 2009. Cognitive deficits in multiple system atrophy correlate with frontal atrophy and disease duration. European Journal of Neurology 16, 1144–1150.

Fearnley, J.M., Lees, A.J., 1990. Striatonigral degeneration. A clinicopathological study. Brain 113, 1823–1842.

Gilman, S., Wenning, G.K., Low, P.A., Brooks, D.J., Mathias, C.J., Trojanowski, J.Q., Wood, N.W., Colosimo, C., Dürr, A., Fowler, C.J., Kaufmann, H., Klockgether, T., Lees, A., Poewe, W., Quinn, N., Revesz, T., Robertson, D., Sandroni, P., Seppi, K., Vidailhet, M., 2008. Second consensus statement on the diagnosis of multiple system atrophy. Neurology 71, 670–676.

Jellinger, K.A., Seppi, K., Wenning, G.K., 2005. Grading of neuropathology in multiple system atrophy: proposal for a novel scale. Movement Disorders 20 (Suppl. 12), S29–S36.

Kato, T., Kume, A., Ito, K., Tadokoro, M., Takahashi, A., Sakuma, S., 1992. Asymmetrical FDG-PET and MRI findings of striatonigral system in multiple system atrophy with hemiparkinsonism. Radiation Medicine 10, 87–93.

Klockgether, T., Ludtke, R., Kramer, B., Abele, M., Bürk, K., Schöls, L., Riess, O., Laccone, F., Boesch, S., Lopes-Cendes, I., Brice, A., Inzelberg, R., Zilber, N., Dichgans, J., 1998. The natural history of degenerative ataxia: a retrospective study in 466 patients. Brain 121, 589–600.

Kume, A., Shiratori, M., Takahashi, A., Kato, T., Ito, K., Tadokoro, M., Sakuma, S., 1992. Hemi-parkinsonism in multiple system atrophy: a PET and MRI study. Journal of Neurological Sciences 110, 37–45.

Mamata, H., Mamata, Y., Westin, C.F., Shenton, M.E., Kikinis, R., Jolesz, F.A., Maier, S.E., 2002. High-resolution line scan diffusion tensor MR imaging of white matter fiber tract anatomy. AJNR. American Journal of Neuroradiology 23, 67–75.

Matsuda, H., Mizumura, S., Nemoto, K., Yamashita, F., Imabayashi, E., Sato, N., Asada, T., 2012. Automatic voxel-based morphometry of structural MRI by SPM8 plus diffeomorphic anatomic registration through exponentiated lie algebra improves the diagnosis of probable Alzheimer Disease. AJNR. American Journal of Neuroradiology 33, 1109–1114.

Messina, D., Cerasa, A., Condino, F., Arabia, G., Novellino, F., Nicoletti, G., Salsone, M., Morelli, M., Lanza, P.L., Quattrone, A., 2011. Patterns of brain atrophy in Parkinson's disease, progressive supranuclear palsy and multiple system atrophy. Parkinsonism & Related Disorders 17, 172–176.

Minnerop, M., Specht, K., Ruhlmann, J., Schimke, N., Abele, M., Weyer, A., Wüllner, U., Klockgether, T., 2007. Voxel-based morphometry and voxel-based relaxometry in multiple system atrophy-a comparison between clinical subtypes and correlations with clinical parameters. NeuroImage 36, 1086–1095.

Minnerop, M., Lüders, E., Specht, K., Ruhlmann, J., Schimke, N., Thompson, P.M., Chou, Y.Y., Toga, A.W., Abele, M., Wüllner, U., Klockgether, T., 2010. Callosal tissue loss in multiple system atrophy-a one-year follow-up study. Movement Disorders 25, 2613–2620.

Nieuwenhuys, R., Voogd, J., Huijzen, C.V., 2008. Telencephalon: Basal Ganglia, The Human Central Nervous Systemfourth ed. Springer 427–489.

Ozawa, T., Paviour, D., Quinn, N.P., Josephs, K.A., Sangha, H., Kilford, L., Healy, D.G., Wood, N.W., Lees, A.J., Holton, J.L., Revesz, T., 2004. The spectrum of pathological involvement of the striatonigral and olivopontocerebellar systems in multiple system atrophy: clinicopathological correlations. Brain 127, 2657–2671.

Papp, M.I., Lantos, P.L., 1994. The distribution of oligodendroglial inclusions in multiple system atrophy and its relevance to clinical symptomatology. Brain 117, 235–243.

Quinn, N., 1989. Multiple system atrophy: the nature of the beast. Journal of Neurology, Neurosurgery, and Psychiatry 52, 78–89.

Schulz, J.B., Skalej, M., Wedekind, D., Luft, A.R., Abele, M., Voigt, K., Dichgans, J., Klockgether, T., 1999. Magnetic resonance imaging-based volumetry differentiates idiopathic Parkinson's syndrome from multiple system atrophy and progressive supranuclear palsy. Annals of Neurology 45, 65–74.

Tir, M., Delmaire, C., le Thuc, V., Duhamel, A., Destée, A., Pruvo, J.P., Defebvre, L., 2009. Motor-related circuit dysfunction in MSA-P: usefulness of combined whole-brain imaging analysis. Movement Disorders 24, 863–870.

Tzarouchi, L.C., Astrakas, L.G., Konitsiotis, S., Tsouli, S., Margariti, P., Zikou, A., Argyropoulou, M.I., 2010. Voxel-based morphometry and voxel-based relaxometry in parkinsonian variant of multiple system atrophy. Journal of Neuroimaging 20, 260–266.

Wenning, G.K., Tison, F., Elliott, L., Quinn, N.P., Daniel, S.E., 1996. Olivopontocerebellar pathology in multiple system atrophy. Movement Disorders 11, 157–162.

Wenning, G.K., Tison, F., Ben Shlomo, Y., Daniel, S.E., Quinn, N.P., 1997. Multiple system atrophy: a review of 203 pathologically proven cases. Movement Disorders 12, 133–147.

Wenning, G.K., Seppi, K., Tison, F., Jellinger, K., 2002. A novel grading scale for striatonigral degeneration (multiple system atrophy). Journal of Neural Transmission 109, 307–320.

Neuroradiology
DOI 10.1007/s00234-013-1138-9

DIAGNOSTIC NEURORADIOLOGY

Discrimination of dementia with Lewy bodies from Alzheimer's disease using voxel-based morphometry of white matter by statistical parametric mapping 8 plus diffeomorphic anatomic registration through exponentiated Lie algebra

Tomoya Nakatsuka · Etsuko Imabayashi · Hiroshi Matsuda · Ryuji Sakakibara · Tsutomu Inaoka · Hitoshi Terada

Received: 19 October 2012 / Accepted: 4 January 2013

Abstract
Introduction The purpose of this study was to identify brain atrophy specific for dementia with Lewy bodies (DLB) and to evaluate the discriminatory performance of this specific atrophy between DLB and Alzheimer's disease (AD).
Methods We retrospectively reviewed 60 DLB and 30 AD patients who had undergone 3D T1-weighted MRI. We randomly divided the DLB patients into two equal groups (A and B). First, we obtained a target volume of interest (VOI) for DLB-specific atrophy using correlation analysis of the percentage rate of significant whole white matter (WM) atrophy calculated using the Voxel-based Specific Regional Analysis System for Alzheimer's Disease (VSRAD) based on statistical parametric mapping 8 (SPM8) plus diffeomorphic anatomic registration through exponentiated Lie algebra, with segmented WM images in group A. We then evaluated the usefulness of this target VOI for discriminating the remaining 30 DLB patients in group B from the 30 AD patients. *Z* score values in this target VOI obtained from VSRAD were used as the determinant in receiver operating characteristic (ROC) analysis.
Results Specific target VOIs for DLB were determined in the right-side dominant dorsal midbrain, right-side dominant dorsal pons, and bilateral cerebellum. ROC analysis revealed that the target VOI limited to the midbrain exhibited the highest area under the ROC curves of 0.75.
Conclusions DLB patients showed specific atrophy in the midbrain, pons, and cerebellum. Midbrain atrophy demonstrated the highest power for discriminating DLB and AD. This approach may be useful for determining the contributions of DLB and AD pathologies to the dementia syndrome.

Keywords Dementia with Lewy bodies (DLB) · Alzheimer's disease (AD) · Statistical parametric mapping (SPM) · Voxel-based morphometry (VBM) · Voxel-based specific regional analysis system for Alzheimer's disease (VSRAD)

Abbreviations

AD	Alzheimer's disease
AUC	Areas under curve
DARTEL	Diffeomorphic anatomical registration through exponentiated Lie algebra
DLB	Dementia with Lewy bodies
GM	Gray matter
H/M	Heart-to-mediastinum

T. Nakatsuka (✉) · T. Inaoka · H. Terada
Department of Radiology, Toho University Sakura Medical Center, 564-1, Shimoshizu, Sakura, Chiba 285-8741, Japan
e-mail: gh23fhuw7@yahoo.co.jp

E. Imabayashi
Department of Nuclear Medicine, Saitama Medical University International Medical Center, Hidaka, Saitama, Japan

H. Matsuda
Integrative Brain Imaging Center, National Center of Neurology and Psychiatry, Kodaira, Tokyo, Japan

R. Sakakibara
Division of Neurology, Department of Internal Medicine, Toho University Sakura Medical Center, Sakura, Chiba, Japan

Published online: 16 January 2013

MIBG	Meta-iodobenzylguanidine
MMSE	Mini-mental state examination
PDD	Parkinson's disease with dementia
PET	Positron emission tomography
ROC	Receiver operating characteristic
SD	Standard deviation
SPECT	Single photon emission computed tomography
SPM	Statistical parametric mapping
TE	Echo time
TI	Inversion time
TR	Repetition time
VBM	Voxel-based morphometry
VOI	Volume of interest
VSRAD	Voxel-based specific regional analysis system for Alzheimer's disease
WM	White matter

Introduction

Dementia with Lewy bodies (DLB) is the second most common type of degenerative dementia, accounting for up to 30 % of all cases of dementia [1]. In addition to dementia, visual hallucinations, fluctuating cognitive impairment, and parkinsonism are the main symptoms [2]. DLB is pathologically characterized by alpha-synuclein inclusions in the brainstem, subcortical nuclei, limbic, and neocortical areas [2]. Although the temporal sequence of symptoms and clinical features of DLB are considered to be different from those of Parkinson's disease with dementia (PDD), discriminating PDD and DLB is difficult in many cases. The accumulation of abnormal neuronal alpha-synuclein inclusions is the defining pathological process common to both PDD and DLB [3]. In this study, PDD and DLB are dealt with as a single pathogenic Lewy body disorder.

Nuclear medicine studies of the dopaminergic system are best suited for detecting pathological states in DLB. One of the more effective examinations for the differential diagnosis of DLB from Alzheimer's disease (AD) is ^{123}I-MIBG myocardial scintigraphy. Yoshita et al. found that the delayed heart-to-mediastinum uptake (H/M) ratio had a sensitivity of 100 %, a specificity of 100 %, and a positive predictive value of 100 % [4]. However, it should be noted that a decreased myocardial MIBG uptake is not specific of DLB; in fact, various heart diseases and diabetes may damage the postganglionic sympathetic neurons, leading to false-positive MIBG findings [5]. Hypometabolism or hypoperfusion in the occipital cortex are also useful for distinguishing DLB from AD [6–8], although their accuracies are not so high. Commonly, MRI has been used to rule out other diseases manifesting dementia, such as cerebral infarction, chronic subdural hematoma, or normal pressure hydrocephalus, and this equipment is more widely used without radionuclides or radiation exposure, as is the case with positron emission tomography (PET) or single photon emission computed tomography (SPECT).

Voxel-based morphometry (VBM), which objectively assesses whole brain structure with voxel-by-voxel comparisons, has been developed to analyze tissue concentrations or volumes between subject groups to distinguish degenerative diseases with dementia [9]. Some studies comparing gray matter (GM) loss in DLB with that of AD by means of VBM have shown similar losses with relative preservation of the temporal lobes in DLB [10–12]. One study with a relatively large number of subjects found greater GM atrophy of the dorsal midbrain in DLB than in AD [12], while others have shown significant atrophy in specific subcortical regions, such as the putamen [13] and basal forebrain [14, 15].

Recently, the statistical parametric mapping 8 (SPM8) plus diffeomorphic anatomical registration through exponentiated Lie algebra (DARTEL; Wellcome Trust Centre for Neuroimaging, London, UK) method was developed for precise VBM [16] for both GM and white matter (WM). DARTEL was shown to improve registration and to provide precise, accurate localization of structural damage and functional overlays. However, Takahashi et al. showed no DLB-specific atrophy of WM compared to AD using SPM8 plus DARTEL [17]. The authors have insisted the GM attenuation in deep brain GM, including the dorsal midbrain, detected in previous studies may be attributed to incomplete registration to the template.

There have been only a few studies evaluating WM changes in DLB compared to AD and healthy controls with VBM [17, 18]. One conventional VBM study using SPM5 for analysis showed significant atrophy of WM in the pons and medulla oblongata in idiopathic Parkinson's disease compared to healthy controls [18]. The other study using SPM8 plus DARTEL for analysis showed no DLB-specific significant atrophy of WM compared to AD [17].

The purpose of our study was to identify a DLB-specific atrophy using SPM8 plus DARTEL and to evaluate the performance of this specific focal atrophy to discriminate between DLB and AD. Although the previous SPM8 plus DARTEL study did not find any DLB-specific atrophy [17], a recent study of antemortem MRI and postmortem neuropathologic classification of DLB and AD revealed that antemortem dorsal mesopontine atrophy was indicative of a high likelihood of DLB [19], leading us to take notice of brain stem

atrophy in DLB. Because SPM8 plus DARTEL classifies most brain stem structures as white matter [16], we focused on white matter changes in the present study.

Materials and methods

We retrospectively reviewed 60 patients with DLB (32 men and 28 women, 77.3±5.8 years of age) and 30 patients with AD (7 men and 23 women, 76.7±5.7 years of age), who had undergone 3D T1-weighted structural MRI from October 2009 to August 2011. All of the 60 patients with DLB had dementia and spontaneous features of parkinsonism. Mini-mental state examination (MMSE) scores were 20.8±4.1 (mean ± SD). Some of them had fluctuating cognition with pronounced variations in attention and alertness, recurrent visual hallucinations that were typically well formed and detailed; thus, they were diagnosed as possible/probable DLB on the basis of the criteria proposed in the consortium on DLB international workshop [2]. All of the 60 patients with DLB revealed reduced H/M ratios on delayed phase of ^{123}I-MIBG myocardial scintigraphy which was used as an adjunct of differential diagnosis of DLB and AD. The 30 patients with AD were diagnosed as probable AD according to the National Institute of Neurologic and Communicative Disorders and Stroke and the Alzheimer's Disease and Related Disorders Association criteria [20, 21]. The MMSE scores of the 30 AD patients were 20.4±4.1. All of AD patients did not reveal reduced H/M ratios on either early or delayed phases of ^{123}I-MIBG myocardial scintigraphy. The ethics committee of Toho University Sakura Medical Center approved this study and all subjects provided informed consent to participate. None of them had asymptomatic cerebral infarction detected by T2-weighted MRI.

All 90 patients underwent MRI examinations on a 1.5T Gyroscan (Philips, Best, the Netherlands). One hundred eighty 3D sections of a T1-weighted, magnetization-prepared rapid acquisition of gradient-echo (MPRAGE) sequence were obtained in a sagittal orientation as 1-mm thick gapless sections (FOV 240 mm, TR 9.7 ms, TE 4.6 ms, flip angle 10°, and TI 525 ms).

Using a free software program, the voxel-based specific regional analysis system for Alzheimer's disease (VSRAD) based on SPM8 plus DARTEL [22], we classified MRIs of all 90 patients into GM, WM, or cerebrospinal fluid images using a unified tissue-segmentation procedure after image-intensity nonuniformity correction, anatomically standardized to a customized template of WM, and then smoothed using an 8-mm full width at half maximum isotropic Gaussian kernel. This new VSRAD software was upgraded from the previous SPM2 version [23]. VSRAD provides statistical Z score images for WM atrophy in each of the patients compared to that of the "normal" database of WM. The Z score was defined as: ([control mean]−[individual value])/(control SD). The "normal" database bundled with VSRAD comprised 80 healthy volunteers (37 men and 43 women), aged 54 to 86 years who underwent 3D T1-weighted MPRAGE sequence using a 1.5T Siemens Vision Plus scanner (Siemens, Erlangen, Germany). Their performance was within normal limits both on the Wechsler Memory Scale—Revised and Wechsler Adult Intelligence Scale—Revised [22]. Their MMSE scores ranged from 26 to 30; 29.1±1.2.

We divided the 60 patients with DLB into two groups at random (group A: 30 patients, group B: 30 patients). We obtained extent of significant WM atrophy for the whole brain, that is, the percentage rate of the coordinates with a Z value exceeding the threshold value of 2 in the whole brain, in each patient as compared with that of the "normal" database bundled with VSRAD in group A. Then, to detect target volumes of interest (VOI) for DLB correlation, we compared this whole brain percentage rate of WM atrophy with that of each voxel in the anatomically standardized and smoothed WM images in group A using SPM8 and their ages as a nuisance covariate. Global nuisance effects were accounted for by including the global covariate as a nuisance effect. The resulting set of values for each contrast of negative or positive correlation constituted statistical parametric maps of the t statistic SPM {t}. Main effects used whole-brain analyses with an uncorrected threshold at voxel level of $p<0.001$ and a cluster false discovery rate for the multiple comparison correction.

We then evaluated the usefulness of this target VOI for discriminating the remaining 30 DLB patients in group B from the 30 AD patients. VSRAD provided statistical Z score images for WM atrophy in each of the patients compared to that of the "normal" database of WM. We obtained

Table 1 Regions in which WM negatively correlated with percentage of whole WM atrophy in 30 DLB patients with DLB (group A)

Brain region	Talairach coordinates				t value
	Side	x	y	z	
Cerebellum posterior lobe	Rt	12	−52	−31	4.5
Cerebellum anterior lobe	Lt	−12	−42	−21	3.9
Midbrain	Rt	4	−24	−11	3.4
Pons	Rt	4	−39	−33	3.2